Theory and experimental investigations on the effect of the halogenated chain of new synthesis compounds based on benzimidazole derivatives on the inhibition corrosion of mild steel in acid media

M. Bouziani Idrissi,[1]* H. Hailou,[1] I. Filali,[1] M. Rbaa,[2] F. Benhiba,[3,4] K. Nouneh,[5] E. El Kafsaoui,[1] C. El Mahjoub,[5] A. El Midaoui,[1] H. Oudda[1] and A. Zarrouk[4]**

[1]*Advanced Materials and Process Engineering Laboratory, Faculty of Science, Ibn Tofail University, P.O. Box 133, Kenitra, Morocco*
[2]*Laboratory of Organic Chemistry, Catalysis and Environment, Faculty of Sciences, Ibn Tofail University, PO Box 133, 14000, Kenitra, Morocco*
[3]*Higher Institute of Nursing Professions and Health Techniques of Agadir, Annex Guelmim, Morocco*
[4]*Laboratory of Materials, Nanotechnology and Environment, Faculty of Sciences, Mohammed V University in Rabat, Av. Ibn Battuta. P.O. Box 1014, Rabat, Morocco*
[5]*Laboratory of Materials Physics & Subatomics, Faculty of Science, Ibn Tofail University, P.O. Box 133, Kenitra, Morocco*
**E-mail: mohammed.bouziani@uit.ac.ma*,
***E-mail: azarrouk@gmail.com*

Abstract

In this study, the behavior of mild steel (MS) corrosion in hydrochloric acid (HCl) solutions in the presence of two new compounds, namely 2-(4-bromophenyl)-1-(2-chloroethyl)-1*H*-benzo-[d]imidazole (24B12CBI) and 1-(2-chloroethyl)-2-(4-chlorophenyl)-1*H*-benzo[d]imidazole (12C24CBI), was investigated. To analyze the inhibitory effects of these substances, several analytical techniques such as electrochemical tests, scanning electron microscopy (SEM) combined with energy-dispersive X-ray (EDX) analysis, atomic force microscopy (AFM), and theoretical approaches (DFT and molecular dynamics) were used. The findings of the experiments showed that both 24B12CBI and 12C24CBI efficiently reduced MS corrosion in 1 M HCl, with a remarkable inhibition level of 90% at a concentration of 10^{-3} M. The inhibitory mechanism was bifurcated, affecting both the anodic and cathodic processes. Electrochemical impedance spectroscopy (EIS) analysis revealed the presence of a singular loop in the diagrams, with an increase in loop size corresponding to higher inhibitor concentrations. This observation suggested the formation of a protective layer upon the metal surface. Furthermore, the 24B12CBI and 12C24CBI inhibitors exhibited minimal temperature dependence and the polarization resistance increased with time. SEM/EDX and AFM investigations confirmed the presence of a protective layer on the surface of the MS, lending credence to the electrochemical findings. Overall, the compounds 24B12CBI and 12C24CBI show significant potential as

corrosion inhibitors (CIs) for MS in 1 M HCl solutions. These findings contribute to a deeper understanding of the inhibition mechanism and highlight the importance of these compounds for mitigating corrosion damage in acidic environments. Data of the theoretical approaches confirm experimental results.

Keywords: *imidazole, MS, HCl, inhibition performance, SEM/AFM, DFT/Molecular dynamics.*

Received: August 24, 2023. Published: October 12, 2023 doi: 10.17675/2305-6894-2023-12-4-8

1. Introduction

MS is widely employed in various industrial applications because of its exceptional structural and mechanical characteristics [1, 2]. However, its susceptibility to corrosion in acidic liquids, which are widely employed in industrial operations widely employed in industrial operations such as Pickling, ore production, boiler cleaning, industrial cleaning, acid descaling, and petrochemical processes, poses a significant challenge [1, 3]. To address this issue, researchers have explored several corrosion protection methods, broadly categorized as surface potential alteration and modification of the metal itself [4, 5].

Surface potential alteration methods include cathodic and anodic protection, which involves manipulating the electrode potential [6]. Alternatively, the metal can be modified by applying either sacrificial or noble metal coatings, or by selecting a more corrosion-resistant alloy [7, 8]. However, Material selection is sometimes hampered by the requirement to preserve other desired features, such as mechanical strength, as well as economic considerations [9]. In such scenarios, CIs offer a viable solution by modifying the corrosive environment [10, 11]. CIs have emerged as the most effective and cost-efficient approach for protecting and preventing steel corrosion [12, 13].

CIs can impact either anodic or cathodic corrosion processes by building protective layer on the steel surface via adsorption [3, 14]. Organic compounds having high electronegativity functional groups, conjugated double or triple bonds with π-electrons, or aromatic rings have shown enhanced corrosion-inhibitory characteristics [13–15]. Functional groups containing heteroatoms, such as sulfur, nitrogen, or oxygen, which possess free lone pairs of electrons, also play an important function in inhibition as well. The combination of these features enhances the inhibition efficiency [13–15]. Recent studies have focused on novel organic compounds, such as pyrazole, triazole, triazepine carboxylate, tetrazole, imidazopyridine, and imidazole, as CIs. Imidazole has garnered significant interest in the realm metallic corrosion prevention owing to its favorable characteristics, affordability, and ease of synthesis [16–19].

Imidazole and its derivatives have garnered significant attention as highly efficient organic inhibitors due to their versatile biological, chemical, and pharmaceutical properties [20, 21]. These derivatives, known as “green” CIs, have previously been demonstrated to be effective in inhibiting corrosion in HCl environments. The inhibitory action of imidazole

derivatives primarily stems from their ability to adsorb onto metallic surfaces, thereby suppressing electrochemical reactions involved in the corrosion process [16, 22, 23].

The present study focuses on synthesizing and characterizing two novel imidazole derivatives namely 24B12CBI and 12C24CBI as CIs for MS in a 1 M HCl solution. This investigation encompasses a comprehensive range of techniques, including scanning electron microscopy (SEM), atomic force microscopy (AFM), quantum chemical calculations, electrochemical impedance spectroscopy (EIS), and potentiodynamic polarization (PDP). These techniques were employed to gain insights into the inhibitory performance and mechanisms of these imidazole derivatives at the molecular and macroscopic levels.

2. Experimental Part

2.1. Molecular structure of tested inhibitors

Selected inhibitors are depicted in Figure 1, these inhibitors possess nucleophilic sites, such as nitrogen, bromine, and chlorine. These different sites may be responsible for the inhibitory performance of these two derivatives.

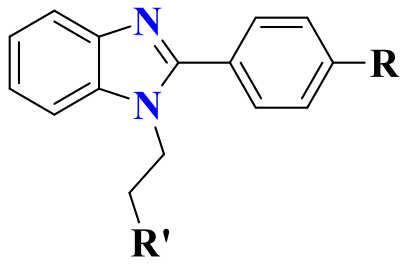

R=Cl, R'= Cl: 12C24CBI
R=Br, R'= Cl: 24B12CBI

Figure 1. Molecule structures of 12C24CBI and 24B12CBI.

2.2. Material and studied media preparation

For the electrochemical tests, MS samples with an exposed surface area of approximately 1 cm^2 were utilized. Before conducting any experiments, the samples underwent wire-electrode cutting and were subsequently ground using a series of SiC abrasive papers ranging from grades 180 to 5000. They were then rinsed with deionized water, degreased with acetone, and dried naturally. A three-electrode cell with an MS sample as the working electrode, platinum as the counter electrode, and a saturated calomel electrode (SCE) as the reference electrode was used in the experiment. To prepare acidic media for testes, deionized water and 35% HCl were used to make a 1 mol/L HCl solution.

2.3. Electrochemical measurements

The electrochemical tests were conducted at 298 K using the three-electrode cell and a ZIVE SP1 electrochemical workstation. During the experiment, the MS electrode was immersed in an acid solution, with and without inhibitors, during 1800 s for the open-circuit potential (OCP) test. The EIS measurements were carried out by applying an AC signal with an amplitude of 5 mV at the OCP value. The frequency range for the EIS analysis was 100 kHz to 10 mHz.

Subsequently, the PDP test was performed within a range from –0.8 to +0.6 V relative to the OCP values, using a scan rate of 0.001 V/s. This test aimed to analyze the electrochemical response of the system under varying potentials to determine the corrosion behavior and polarization characteristics.

The inhibition efficiency from the Tafel curves (η) was determined as follows:

$$\eta_{\mathrm{PDP}} = \frac{i_{\mathrm{corr}} - i'_{\mathrm{corr}}}{i_{\mathrm{corr}}} \cdot 100 \tag{1}$$

where i_{corr} and i'_{corr} are the corrosion current densities without and with the inhibitor, respectively.

$$\eta_{\mathrm{EIS}} = \frac{R_{\mathrm{p}} - R_{\mathrm{p}}^{0}}{R_{\mathrm{p}}} \cdot 100 \tag{2}$$

where R_{p}^{0} and R_{p} are the polarization resistance values without and with the presence of inhibitors, respectively.

2.3. SEM/EDX and AFM analysis

The SEM micrographs of the specimens were acquired using a Quanta FEG 450 instrument. To prepare for this analysis, MS samples measuring 1.0 cm × 1.0cm × 0 cm were meticulously abraded using various grades of emery papers. Subsequently, the samples were thoroughly rinsed with double-distilled water and acetone. Once dried, the samples were immersed in 1 M HCl solutions, both with and without 10^{-3} mol/L of inhibitors. This immersion was performed at 298 K for 12 hours. SEM micrographs were captured to examine the morphological characteristics.

Atomic Force Microscopy (AFM) was performed at 298 K for samples prepared in the same conditions (as the SEM technique) to further investigate the morphology of the deposited layers. AFM micrographs were obtained using a Veeco Dimension ICON system (Bruker).

2.4. Computational details

2.4.1. Density functional theory calculations

Quantum-based approaches have become increasingly valuable for establishing connections between molecular structural descriptors and their inhibitory performance. Therefore, the Density Functional Theory (DFT) method was employed using the Gaussian 09 program with the B3LYP and 6-311G++(d,p) basis set [24].

This computational approach allowed for the determination of several theoretical descriptors, including the energies of lowest unoccupied molecular orbital (E_{HOMO}) and highest occupied molecular orbital (E_{LUMO}), energy gap (ΔE), dipole moment (μ), hardness (η), softness (σ), electronegativity (χ), electrophilic index (ω), nucleophilic index (ε), fraction of electrons transferred (ΔN), and total energy [25–27].

The equations giving these parameters are as follows:

$$\Delta E = E_{LUMO} - E_{HOMO} \tag{3}$$

$$\chi = -\frac{E_{HOMO} + E_{LUMO}}{2} \tag{4}$$

$$\eta = \frac{E_{LUMO} - E_{HOMO}}{2} \tag{5}$$

$$\sigma = \frac{1}{\eta} \tag{6}$$

$$\omega = -\frac{\chi^2}{2\eta} \tag{7}$$

$$\varepsilon = \frac{1}{\omega} \tag{8}$$

$$\Delta N = \frac{\phi_{Fe} - \chi_{inhibitor}}{2\left(\eta_{Fe} + \eta_{inhibitor}\right)} \tag{9}$$

2.4.2. Molecular dynamics

According to the interatomic interactions involving the inhibitor and the metal, molecular dynamics (MD) simulation is the good method for describing the process of an inhibitor molecule adhering to a metal surface. This simulation was realized using the Forcite module integrated with the Materials Studio/2016 program. The interactions for the tested system were carried out using a simulator box ($27.30 \times 27.30 \times 37.13$ Å^3) with a 6-layer slab for the $Fe_{(110)}$ in each layer corresponding to a unit cell (11×11). By 33 Å^3, the simulation box is entirely empty. This vacuum is filled by 491 H_2O, $9H_3O^+$, $9Cl^-$, and inhibitor. The Andersen thermostat, NVT ensemble set, with a simulating duration of 10^3 ps and a time step of 1 fs, all inside the COMPASS force domain, was employed to regulate the simulation system's temperature, which was set at 298 K [28].

3. Results and Discussion

3.1. Corrosion tests

3.1.1. Potentiodynamic polarization curves

To investigate the electrochemical behavior of 24B12CBI and 12C24CBI as inhibitors and to gain insights into their impact on the kinetics of electrochemical reactions, polarization curves of MS were obtained in 1 M HCl solution with and without different concentrations of the inhibitors. Figure 2 displays the representative cathodic and anodic curves.

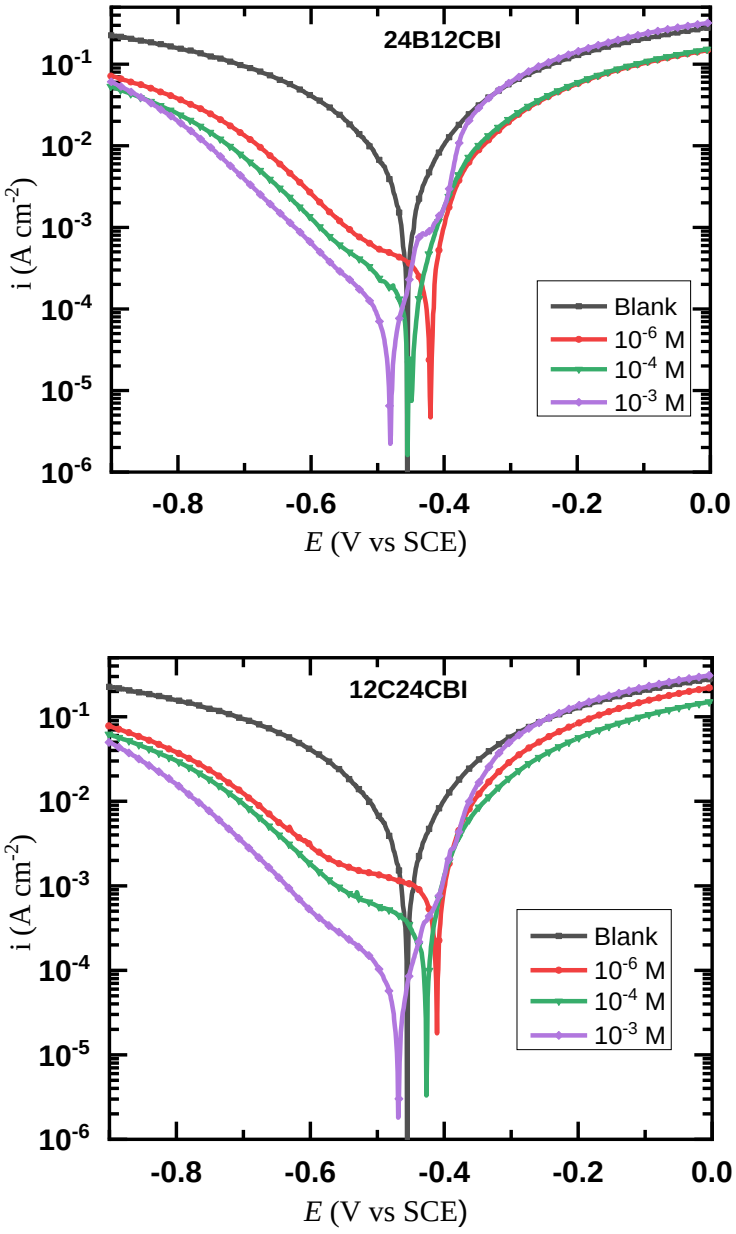

Figure 2. PDP plots of MS in 1 M HCl at diverse concentrations of 24B12CBI and 12C24CBI.

The inclusion of 24B12CBI and 12C24CBI compounds in the 1 M HCl solution led to a reduction in both cathodic and anodic current densities. This inhibitory effect became more pronounced as the inhibitor concentration was increased. These results suggest that organic molecules limit both cathodic hydrogen evolution mechanisms and anodic metal dissolution by occupying active sites on the MS surface through adsorption [29].

The displacements of the cathodic and anodic branches were not uniform with varying concentrations of 24B12CBI and 12C24CBI. The i_{corr} values significantly decreased with increasing inhibitor concentration [30, 31]. This suggests a modification of the cathodic and anodic processes [30]. The presence of heteroatoms (N, Cl, and Br) in the studied molecules, which possess lone pairs, promoted the formation of Fe(II)-24B12CBI and 12C24CBI complexes, thereby altering the iron dissolution mechanism [32].

Table 1 displays electrochemical PDP parameters, such as E_{corr} and i_{corr}. The i_{corr} values were obtained by extrapolating the cathode Tafel lines to the free corrosion potential for inhibited and uninhibited conditions. The best inhibition efficiency was observed at a concentration of 10^{-3} M, with 24B12CBI displaying a 90% efficiency and 12C24CBI displaying 94%.

Table 1. PDP parameters for MS in 1 M HCl with and without various concentrations of 21B12CBI and 12C24CBI at 298 K.

Inhibitor	**Conc. (M)**	**$-E_{corr}$ (mV/SCE)**	**i_{corr} ($\mu A \cdot cm^{-2}$)**	**η_{PDP} (%)**
Blank	1	455.0	887.00	–
24B12CBI	10^{-6}	411.6	408.80	54.0
	10^{-4}	426.6	131.70	85.1
	10^{-3}	391.9	84.70	90.5
12C24CBI	10^{-6}	441.7	150.30	83.1
	10^{-4}	423.2	76.15	91.4
	10^{-3}	455.0	51.80	94.2

The corrosion current densities decreased when inhibitors were added to the corrosive media. This suggests that the corrosion rate decreased as well. The decrease in corrosion current density also led to an increase in polarization resistance, which improved protection against corrosion.

In addition, it was observed that E_{corr} showed a small change (not exceeding 85 mV in any instance) when organic compounds were present. This suggests that 24B12CBI and 12C24CBI can be categorized as mixed inhibitors when used in acidic electrolytes [32].

3.1.2. EIS results

Figure 3 displays the Nyquist plots obtained by the EIS technique. The Nyquist plots revealed the presence of a single capacitive loop, which corresponded to the polarization

resistance (R_p) [32]. The size of the capacitive loops noticeably differed when inhibitors 24B12CBI and 12C24CBI were present. This observation provides evidence of the alteration in the electrochemical behavior and the formation of a protective layer on the surface of MS in the presence of 24B12CBI and 12C24CBI.

Although the semicircles observed in Figure 3 are not perfectly circular, they can be attributed to the heterogeneity of the electrode surface [33]. Surface impurities, roughness, dislocations, and inhibitor adsorption can contribute to this heterogeneity [33]. However, the increase in the size of the capacitive loops with higher inhibitor concentrations indicated the enhanced inhibition performance of the studied compounds.

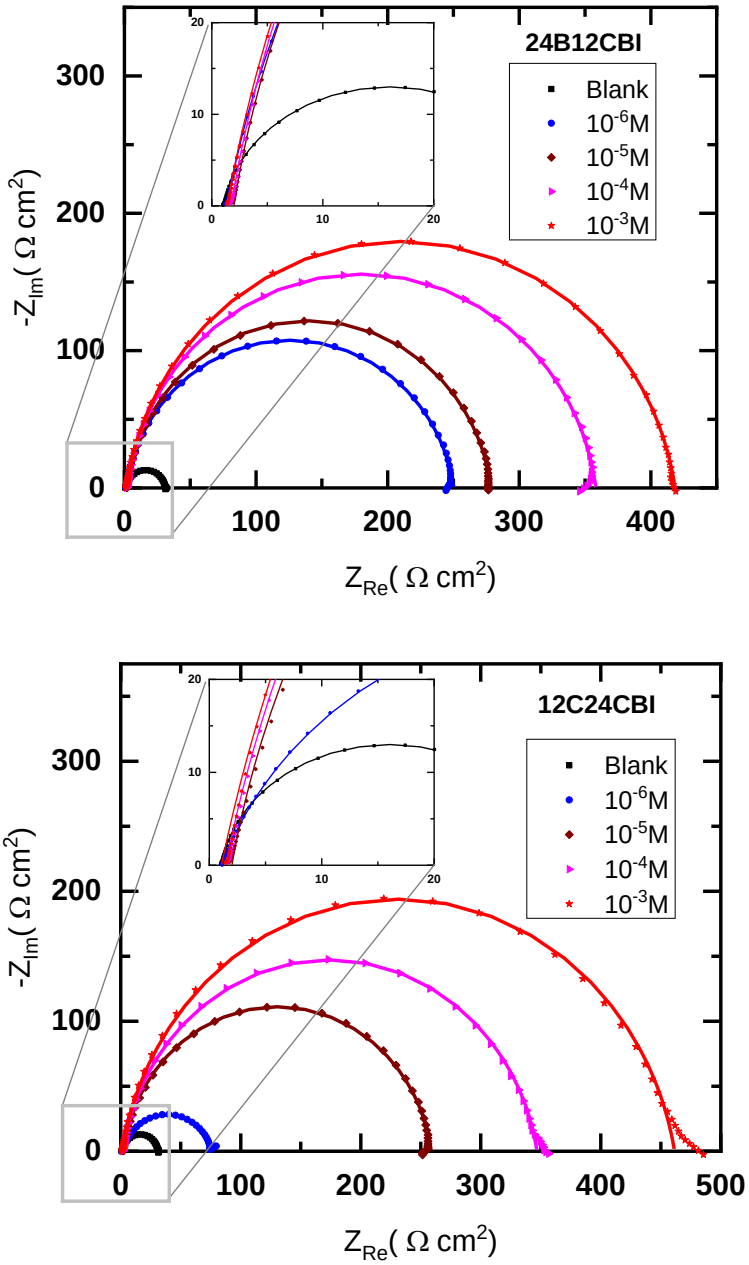

Figure 3. Nyquist plots for MS in 1 M HCl at various contents of 24B12CBI and 12C24CBI.

The Bode phase diagram in Figure 4 shows that only one peak appears in the phase angle frequency relationship curve, corresponding to a reaction process with only a single time constant for both of 24B12CBI and 12C24CBI. The phase angle values increased compared to the blank electrolyte in the case of 24B12CBI and 12C24CBI, proving that both inhibitors can coat the metal surface with a protective layer. Figure 4 shows also that the impedance moduli Z increased significantly after adding inhibitors. The variation of impedance modulus & phase angle is positively correlated with the inhibitors proportion, which means that the more inhibitor deposit onto the electrode to form a protective coating, the more effectively the corrosion reaction is inhibited as inhibitor concentration rises [34, 35].

The electrochemical reaction observed at E_{OCP} can be described by the equivalent electrical circuit (EC) depicted in Figure 5. Different concentrations of the inhibitors were tested using various circuits, and the Nyquist plots obtained using this EC demonstrated a good fit with the experimental data. The EC includes a phase element constant CPE representing the capacitance in parallel with the polarization resistance R_p, both of which are connected in series with the solution resistance R_s. These EIS parameters are reported in Table 2.

Table 2. EIS data for MS in 1 M HCl solution with various concentrations of 24B12CBI and 12C24CBI at 298 K.

Inhibitor	C_{inh} **(M)**	R_s **(Ω·cm²)**	R **(Ω·cm²)**	Q **(μF·S^{n-1})**	n	C_{dl} **(μF·cm^{-2})**	R_p **(Ω·cm²)**	η_{EIS} **(%)**	**θ**
Blank	1	1.060	30.01	1.800	0.91	94.700	28.95	–	–
24B12CBI	10^{-6}	1.252	245.8	0.134	0.89	0.038	244.55	88.2	0.882
	10^{-5}	1.844	276.0	0.088	0.90	0.028	274.12	89.4	0.894
	10^{-4}	1.661	358.9	0.093	0.90	0.029	357.24	91.9	0.919
	10^{-3}	1.374	419.1	0.106	0.89	0.031	417.765	93.1	0.931
12C24CBI	10^{-6}	1.208	74.41	0.295	0.83	0.024	73.202	62.1	0.621
	10^{-5}	1.727	263.02	0.172	0.88	0.042	261.293	88.9	0.889
	10^{-4}	1.597	347.8	0.113	0.89	0.032	346.203	91.6	0.916
	10^{-3}	1.503	458.2	0.106	0.90	0.036	456.697	93.7	0.937

Table 2 shows that when inhibitors are added to a solution, the value of R_P rises from 28.95 Ω·cm² to 417.765 Ω·cm² and to 456.697 Ω·cm² respectively for 24B12CBI and 12C24CBI at 10^{-3} M. The formation of a protective layer at the metal surface interface shows an increase in the R_p value. Consequently, the double-layer capacitance (C_{dl}) underwent a slight decrease, with values ranging from 0.031 to 0.038 μF·cm^{-2} for 24B12CBI and from 0.036 to 0.042 μF cm^{-2} for 12C24CBI as the inhibitor concentration increased. This

reduction in C_{dl} values suggests the adsorption of inhibitor molecules, leading to a decrease in the corrosion process of MS in the hydrochloric acid solution [30, 32]. The obtained inhibition efficiencies support this observation, with 93.1% for 24B12CBI and 93.7% for 12C24CBI at 10^{-3} M.

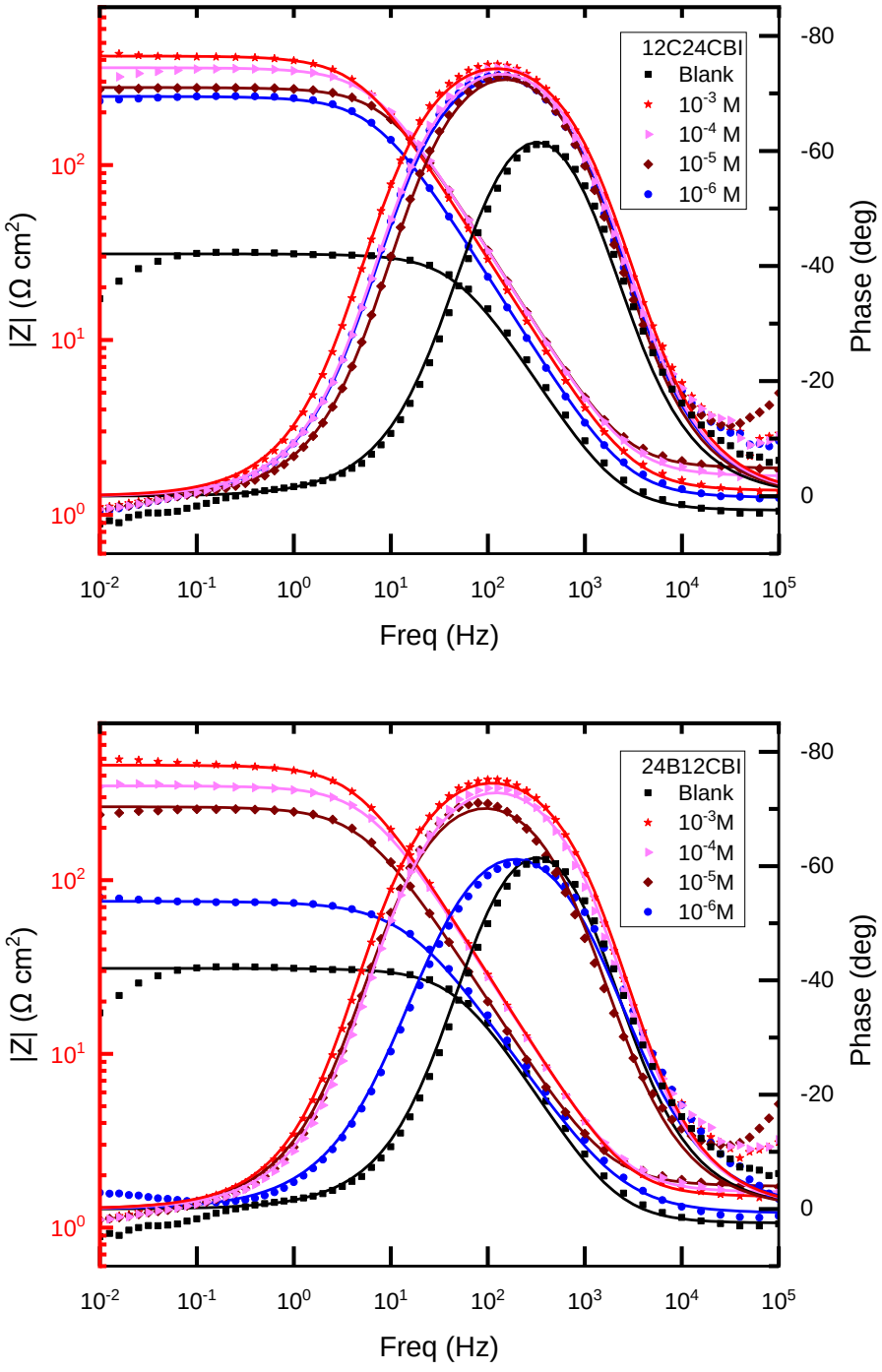

Figure 4. Bode and phase plots for MS in 1 M HCl at various contents of 24B12CBI and 12C24CBI at E_{OCP} (T=298 K).

Figure 5. EC for MS/1 M HCl system.

Furthermore, the inhibition efficiencies obtained from EIS analyses were consistent with those obtained from the PDP technique, confirming the effectiveness of the studied molecules as CIs for MS in a hydrochloric acid medium. According to the information provided, both 24B12CBI and 12C24CBI exhibit similar levels of efficiency as corrosion inhibitors for mild steel (MS) in a hydrochloric acid medium. The inhibition efficiencies obtained from both the polarization resistance (PDP) technique and the electrochemical impedance spectroscopy (EIS) analyses are quite close. Therefore, based on the data given, it's difficult to definitively conclude that one compound is significantly more efficient than the other in terms of corrosion inhibition. Both 24B12CBI and 12C24CBI appear to offer nearly identical levels of protection against corrosion for mild steel in the hydrochloric acid medium under the specified conditions. Among the two compounds, 12C24CBI (the compound containing chlorine) appears to be a little more efficient as a corrosion inhibitor compared to 24B12CBI (the compound containing bromine) [36].

3.1.3. Adsorption process of inhibitor molecules

The adsorption of inhibitors on metal surfaces is accomplished through the replacement of water molecules already present on the surface [37]. It is plausible to posit a direct correlation between the inhibitory effectiveness, denoted as the inhibition efficiency (η_{EIS}), and the extent of surface coverage, represented as θ, as expressed by Equation 10 [37, 38]. The determination of θ for various concentrations of the inhibitors 24B12CBI and 12C24CBI was conducted through the analysis of EIS data, within the context of MS exposed to a 1 M HCl solution at 298 K.

$$\theta = \frac{\eta_{EIS}}{100} \tag{10}$$

To elucidate the adsorption process and understand the reaction of the inhibitor molecule on the metal surface, various adsorption isotherms, such as Temkin, Langmuir, and Frumkin isotherms, have been utilized in similar studies [39, 40]. These isotherms provide valuable information regarding the interaction between the inhibitor and the metal surface. The linear regression coefficient (R^2) closely approaching unity substantiated the Langmuir adsorption model (Table 3). In our case, the observed increase in the inhibition efficiency with increasing inhibitor concentration can be explained as follows:

$$\frac{C_{inh}}{\theta} = C_{inh} + \frac{1}{K_{ads}} \tag{11}$$

where C_{inh} is the inhibitor concentration, θ is the surface coverage, and K_{ads} is the equilibrium constant for the adsorption-desorption process.

The experimental data presented in Figure 6 validates the applicability of this equation to our results. Consequently, the value of K_{ads} was calculated. It is important to note that a high value of K_{ads} indicates strong adsorption efficiency.

Using the calculated value of K_{ads}, the free energy of adsorption (ΔG^0_{ads}) was determined using the following equation:

$$\Delta G^0_{ads} = -RT \ln\left(55.5 K_{ads}\right) \tag{12}$$

where R is the universal gas constant (8.314 $J \cdot K^{-1} \cdot mol^{-1}$), T is the absolute temperature (K), 55.5 is the molar concentration of water ($mol \cdot L^{-1}$).

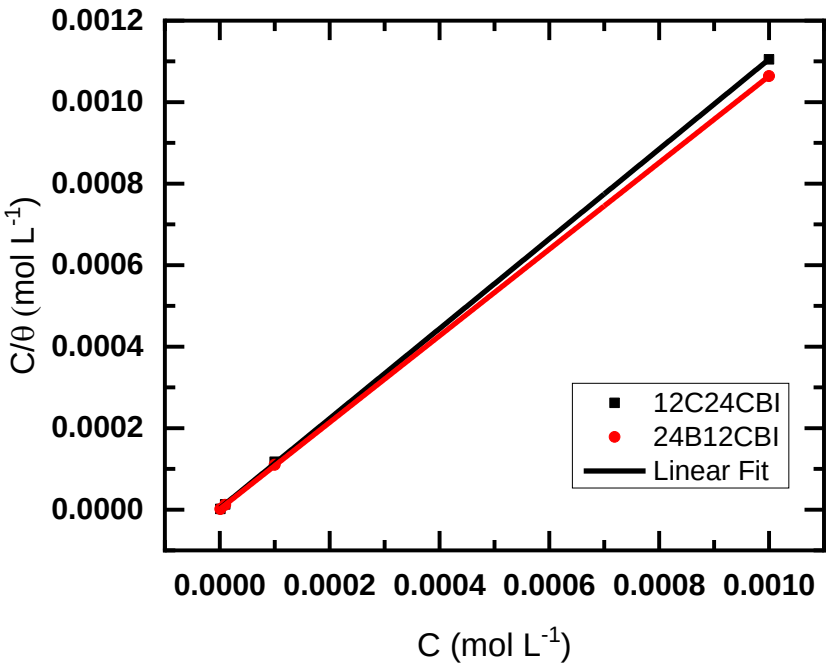

Figure 6. Adsorption isotherm plots for the Langmuir model for various 24B12CBI and 12C24CBI contents at 298 K.

The negative value of ΔG^0_{ads} indicates that the adsorption process occurred spontaneously, resulting in the formation of a protective coating on the metal surface. Generally, absolute values of ΔG^0_{ads} less than 20 suggest physical adsorption, while values greater than 40 indicate chemical bonding and charge transfer (chemisorption) between the organic molecule and metal [39, 40].

In our case, the obtained values of ΔG^0_{ads}, specifically –43.13 kJ/mol for 24B12CBI and –41.34 kJ/mol for 12C24CBI, suggest chemisorption as the dominant mechanism.

Table 3. Curve fitting data of 24B12CBI and 12C24CBI molecule adsorption on the MS surface according to different adsorption isotherms.

Isotherms	Linear forms	Curves	Parameters	Fitting values	
				24B12CBI	12C24CBI
Langmuir	$\frac{C_{inh}}{\theta} = \frac{1}{K_{ads}} + C_{inh}$	$\frac{C_{inh}}{\theta} = f\left(C_{inh}\right)$	R^2	0.9999	0.9996
			K_{ads} ($L \cdot mol^{-1}$)	0.655 $\times 10^6$	0.318 $\times 10^6$
			Slope	1.063	1.102

*Where *f* is the factor of energetic inhomogeneity and the parameter *a* is the number of water molecules replaced by inhibitor molecules on the metallic surface, respectively.

3.1.4. Effect of temperature

Temperature is a parameter that can alter the interactions between a metallic surface and inhibit or uninhibit corrosive electrolyte [39, 41]. Thus, it would be interesting to investigate the efficiency of the inhibitors at different temperatures. To accomplish this, the polarization curve technique (Tafel) was employed at different temperatures. Table 4 shows the polarization data obtained for the optimum concentration (10^{-3} M), and the various electrochemical parameters.

$$i = A\exp\left(-\frac{E_a}{RT}\right) \tag{13}$$

$$i = \frac{RT}{Nh}\exp\frac{\Delta S_a}{R}\exp\left(-\frac{\Delta H_a}{RT}\right) \tag{14}$$

where R, T, h, N, and R_p are the ideal gas constant, absolute temperature, Planck's constant, Avogadro's number, and polarization resistance, respectively.

Table 4. Electrochemical data and inhibition efficiency values for the MS/1 M HCl system with and without 10^{-3} M of inhibitors at diverse temperature values.

	T (K)	i_{corr} ($\mu A \cdot cm^{-2}$)	η_{PDP} (%)
Blank solution	298	887.0	–
	308	984.0	–
	318	1462.0	–
	328	2487.0	–

	T (K)	i_{corr} (μA·cm^{-2})	η_{PDP} (%)
24B12CBI	298	84.7	90.5
	308	265.2	73.1
	318	358.2	75.5
	328	963.7	61.2
12C24CBI	298	51.8	94.2
	308	208.4	78.8
	318	265.2	82.0
	328	579.3	77.0

Figure 7 depicts Arrhenius plots for steel in 1 M HCl solutions with 24B12CBI and 12C24CBI, respectively. The plots show the natural logarithm of i_{corr} plotted against 1000/T as well as the natural logarithm of i_{corr}/T plotted against 1000/T. These plots were generated using the Arrhenius Equation 13 and the transition state Equation 14. Table 5 presents the activation parameters for MS in 1 M HCl, with and without the investigated inhibitor. The results revealed that the studied inhibitor considerably inhibited the corrosion reaction of MS, as the i_{corr} values in its presence were lower than those obtained in the absence of the inhibitor. In addition, it exhibited good inhibition performance at different temperatures. However, the efficiency decreased slightly with increasing temperature.

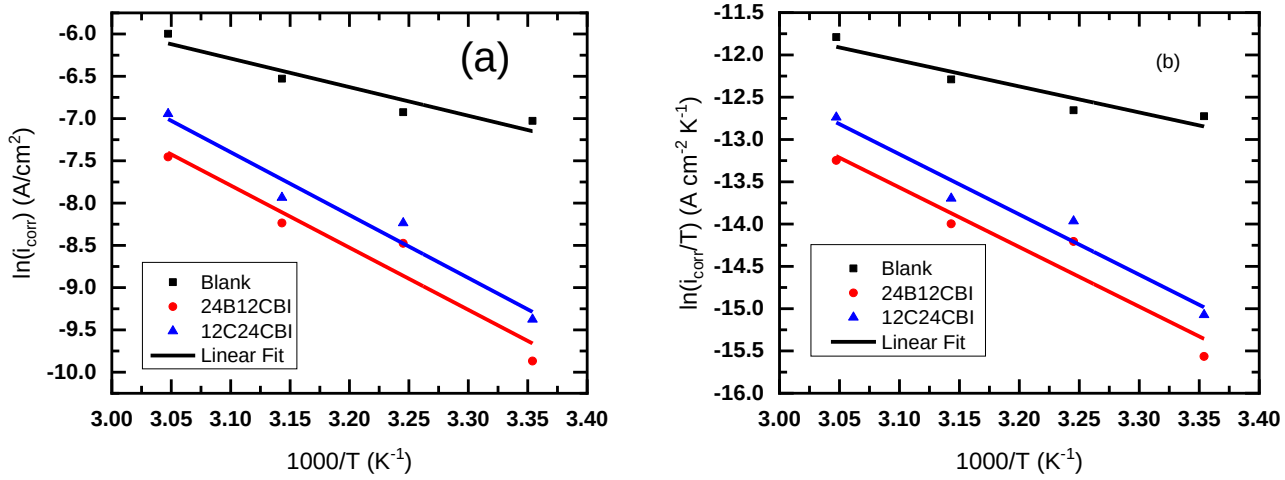

Figure 7. (a) Arrhenius and (b) Transition plots with and without inhibitors for MS/1 M HCl.

Upon examination of the activation parameters, it was evident that the values of E_a (activation energy) in the presence of the investigated inhibitor exceeded those of the blank solution. This observation implies that the inhibitors physically adsorb onto the metal surfaces. The positive values of ΔH_a^* (enthalpy of activation) indicate that the metal

dissolution process is endothermic, necessitating energy input. Additionally, the negative sign of entropy (ΔS_a^*) signifies a decrease in the level of randomness during the conversion of reactants into activated complexes [42, 43].

Table 5. Thermodynamic parameters in the absence and presence of inhibitors for MS/1 M HCl.

	E_a (kJ·mol^{-1})	ΔH (kJ·mol^{-1})	ΔS (J·mol^{-1}·K^{-1})
Blank	28.147	25.55	–218.657
24B12CBI	61.168	58.57	–128.78
12C24CBI	61.833	59.23	–123.45

3.1.5. Influence of immersion time

Figure 8 displays the impedance plots of an MS/1 M HCl system in the presence of 24B12CBI and 12C24CBI at various immersion times, revealing that the polarization resistance values, R_p, increase with time for 24B12CBI; they rise from 148.18 Ω·cm^2 after 1 hour to 248.36 Ω·cm^2 after 4 hours, and then begin to decrease to 239.1 Ω·cm^2 after 12 hours of immersion time, and decrease with time for 12C24CBI, from 388.33 Ω·cm^2 after 1 hour to 289.48 Ω·cm^2 after 12 hours of immersion time. These findings can be attributed to the desorption of molecules from the metal surface [44–46].

Table 6. Electrochemical data and inhibition efficiency values for MS in 1 M HCl with 24B12CBI and 12C24CBI at immersion time.

Inhibitor	Time (h)	R_s (Ω·cm^2)	R_{ad} (Ω·cm^2)	Q_{ad} (μF·cm^{-2})	n_{ad}	R_p (Ω·cm^2)	η_{EIS} (%)
12C24CBI	1	0.967	389.30	0.149	0.792	388.330	92.40
	2	0.966	361.10	0.151	0.792	360.134	91.86
	4	1.063	359.30	0.168	0.787	358.237	91.82
	8	1.110	344.40	0.175	0.784	343.290	91.26
	12	1.120	290.60	0.186	0.784	289.480	89.64
24B12CBI	1	0.890	149.07	0.221	0.813	148.180	80.00
	2	0.741	229.30	0.201	0.823	228.559	87.00
	4	0.839	249.20	0.208	0.818	248.361	88.00
	8	0.947	243.90	0.224	0.812	242.953	87.90
	12	0.904	240.00	0.242	0.804	239.096	87.50

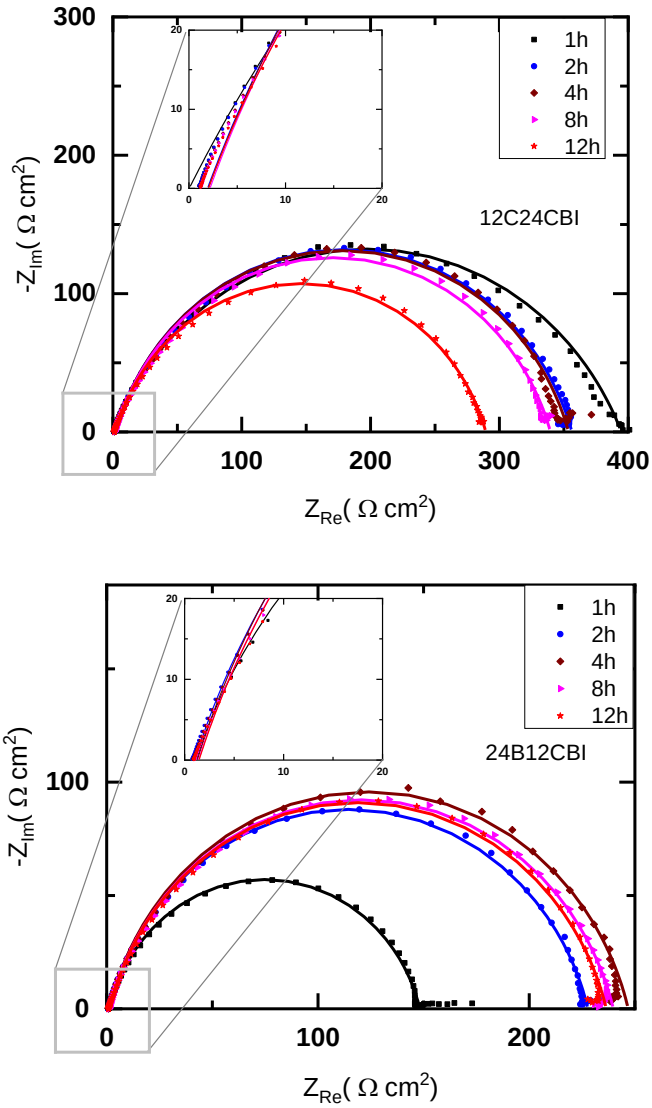

Figure 8. Diagram plots at various immersion times at EOCP for (a) 24B12CBI and (b) 12C24CBI.

3.1.6. SEM/EDX analyses results

Figure 9 shows a comparison of the SEM images and their corresponding EDX spectra obtained for MS samples submerged in an aggressive solution, both with and without 24B12CBI and 12C24CBI. Figure 9 (Blank) illustrates the MS sample after submerging in a 1 M HCl solution in the absence of inhibitors, where in the MS surface is badly corroded, the corresponding EDX data indicate the presence of oxygen due to the formation of corrosion products.

However, in the presence of 24B12CBI and 12C24CBI (Figure 9), the MS surface showed improvement with fewer cracks and pits compared to the blank, and the corresponding EDX spectrum showed a lower presence of oxygen atoms and higher amount of iron atoms, confirming the formation of a protective layer with the adsorption of

molecules onto the surface [45]. Thus, these results confirm the adsorption of the 24B12CBI and 12C24CBI inhibitor molecules on the MS surfaces.

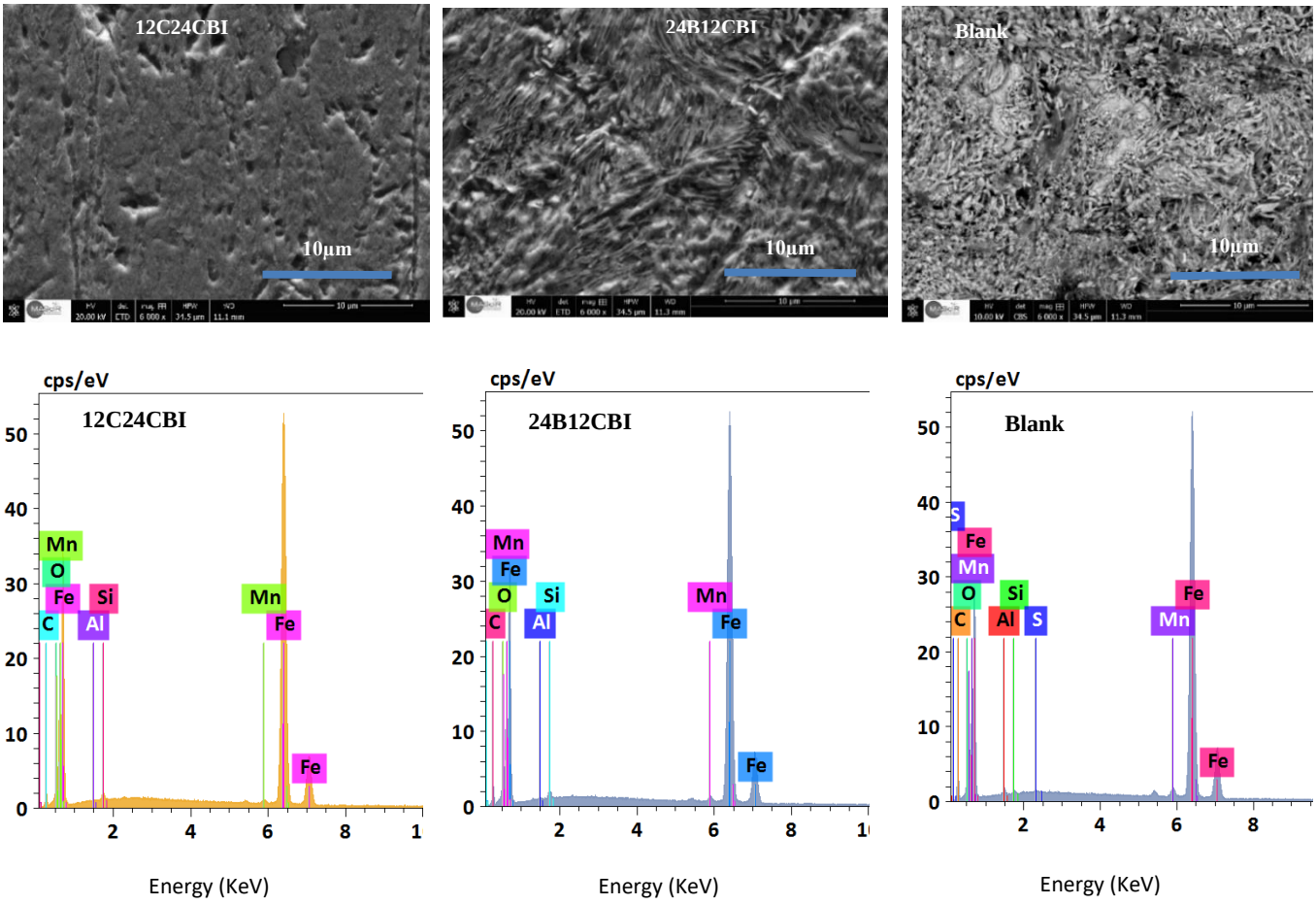

	12C24CBI		24B12CBI		Blank	
	Mass (%)	**Atom (%)**	**Mass (%)**	**Atom (%)**	**Mass (%)**	**Atom (%)**
C	4.36	16.93	6.39	23.16	9.09	29.52
O	0.89	2.60	1.23	3.34	2.79	6.96
Al	0.08	0.13	0.11	0.18	0.49	0.70
Si	0.4	0.66	0.51	0.50	0.11	0.15
S	–	–	–	–	0.12	0.14
Mg	0.79	0.67	0.95	0.75	1.59	1.13
Fe	94.70	79.01	92.10	71.79	86.06	61.40

Figure 9. Micrographs of MS surfaces and EDX data of MS after 12 h of immersion in 1 M HCl with and without 10^{-3} M 24B12CBI and 12C24CBI at 298 K.

3.1.7. AFM analysis

Atomic force microscopy (AFM) analysis is a valuable technique for quantifying the surface roughness of metallic materials [47]. In this study, the metal substrates (MS) were immersed in a corrosive medium without any inhibitors and in the presence of 10^{-3} M 24B12CBI and 12C24CBI at a temperature of 298 K for 12 h. The objective of this study was to investigate the corrosion inhibition properties of these compounds. The surface morphology was examined using atomic force microscopy (AFM), and the results were visualized using 3D-dimensional images (Figure 10).

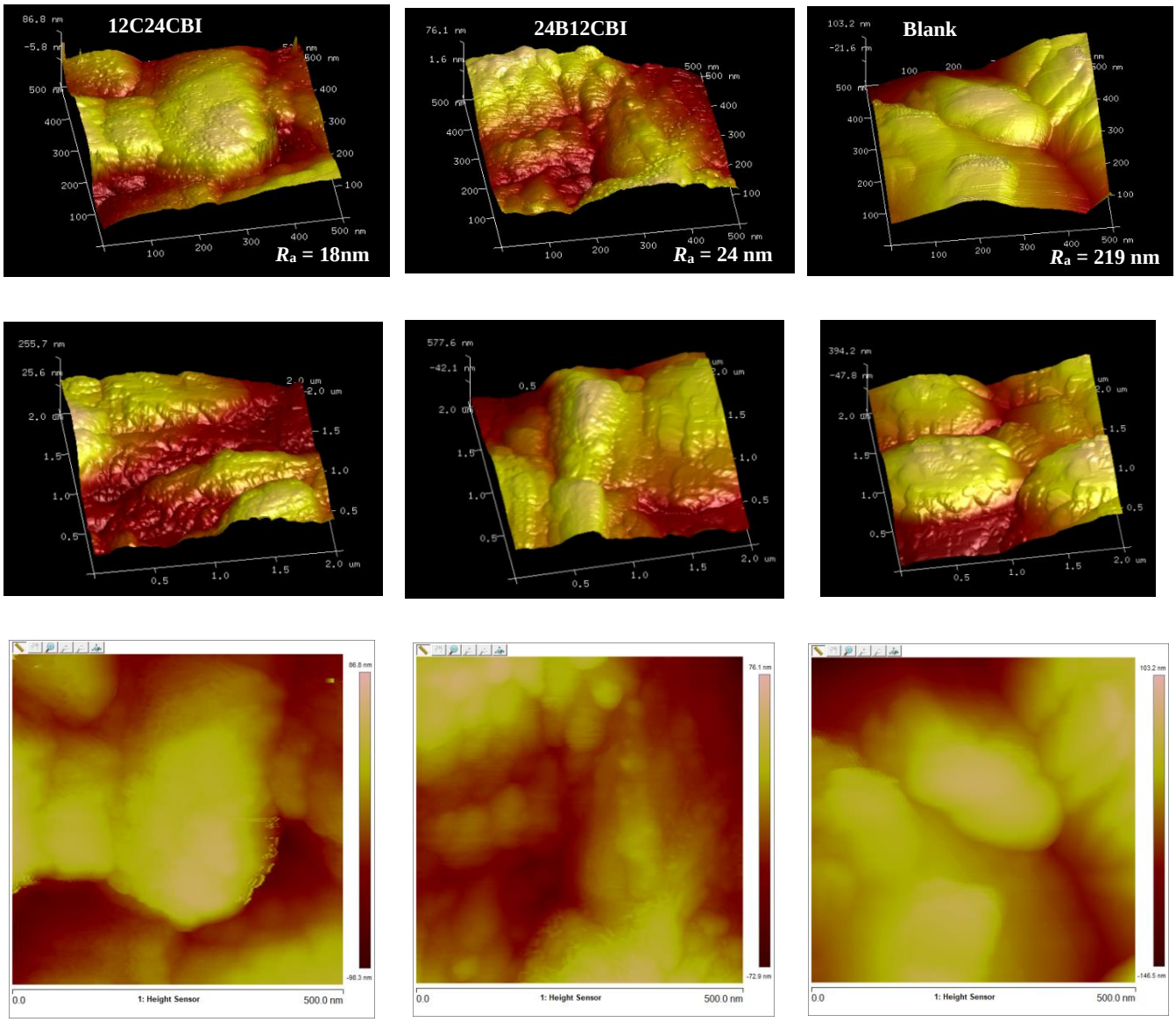

Figure 10. 2D and 3D AFM images after 12 hours of immersion in 1 M HCl with and without 24B12CBI and 12C24CBI inhibitors at 10^{-3} M at 298 K.

An analysis of the AFM images in Figure 10 revealed notable surface damage and the presence of visible corroded pits when the MS substrates were immersed in the corrosive medium alone. These observations suggest the deterioration of the MS due to corrosion. However, upon the addition of the 24B12CBI and 12C24CBI inhibitors, a distinct improvement in the surface conditions was observed. Diagonal section profile of AFM images (Figure 11) show that the treated surfaces exhibited enhanced smoothness, uniformity, and better adhesion, indicating the effectiveness of the inhibitors in mitigating corrosive effects [48].

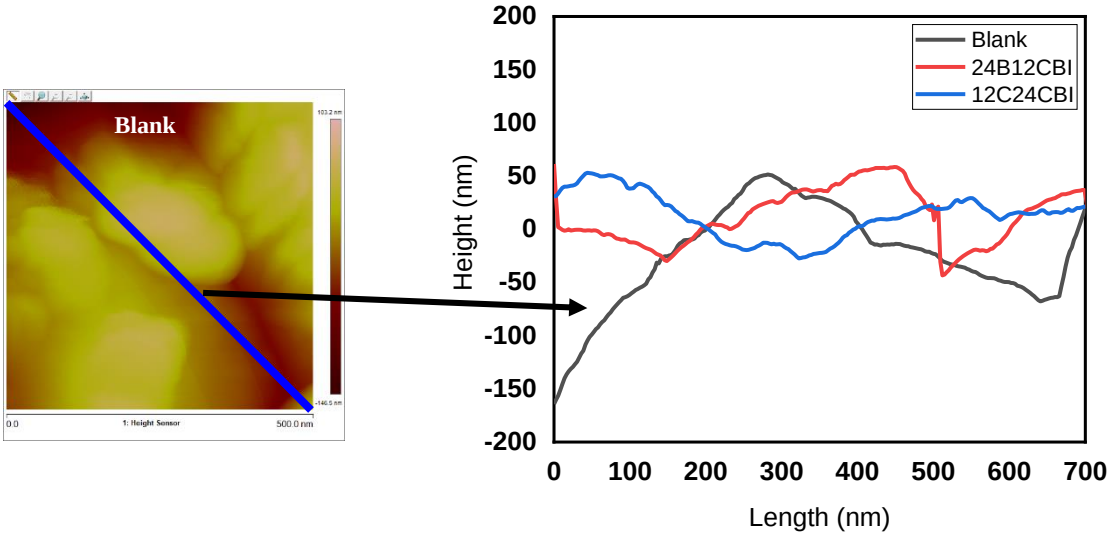

Figure 11. Diagonal section profile of AFM images after 12 hours of immersion in 1 M HCl with and without 24B12CBI and 12C24CBI inhibitors at 10^{-3} M at 298 K.

3.2. Theoretical study

3.2.1. DFT calculations

Density Functional Theory (DFT) is a potent quantum chemical method used to study corrosion inhibition. This helps to establish a correlation between the molecular electronic parameters and their ability to prevent corrosion on metal surfaces. Additionally, it can facilitate the understanding of the mechanism that occurs between these inhibitors and the steel surface. Figure 13 displays the optimized structures, HOMO and LUMO electron density distributions, and electrostatic surface potential (ESP) of the studied molecules. The descriptors used are listed in Table 7.

Based on the findings in Figure 12, it is evident that 24B12CBI and 12C24CBI have HOMO density distributions centered primarily on the C=C, C=N, C–N, C–Br, and C–Cl bonds. Conversely, the LUMO density distribution was mainly localized on the benzene ring. Additionally, Electrostatic Potential Surfaces (ESP) provide insights into the electrophilic active sites of molecular structures. These ESP maps suggest that the electrophilic active site is localized around the atoms of benzene, the carbon linked to the

nitrogen atom, and Cl and Br linked to benzene. This is indicated by the dark blue color observed in the ESP maps.

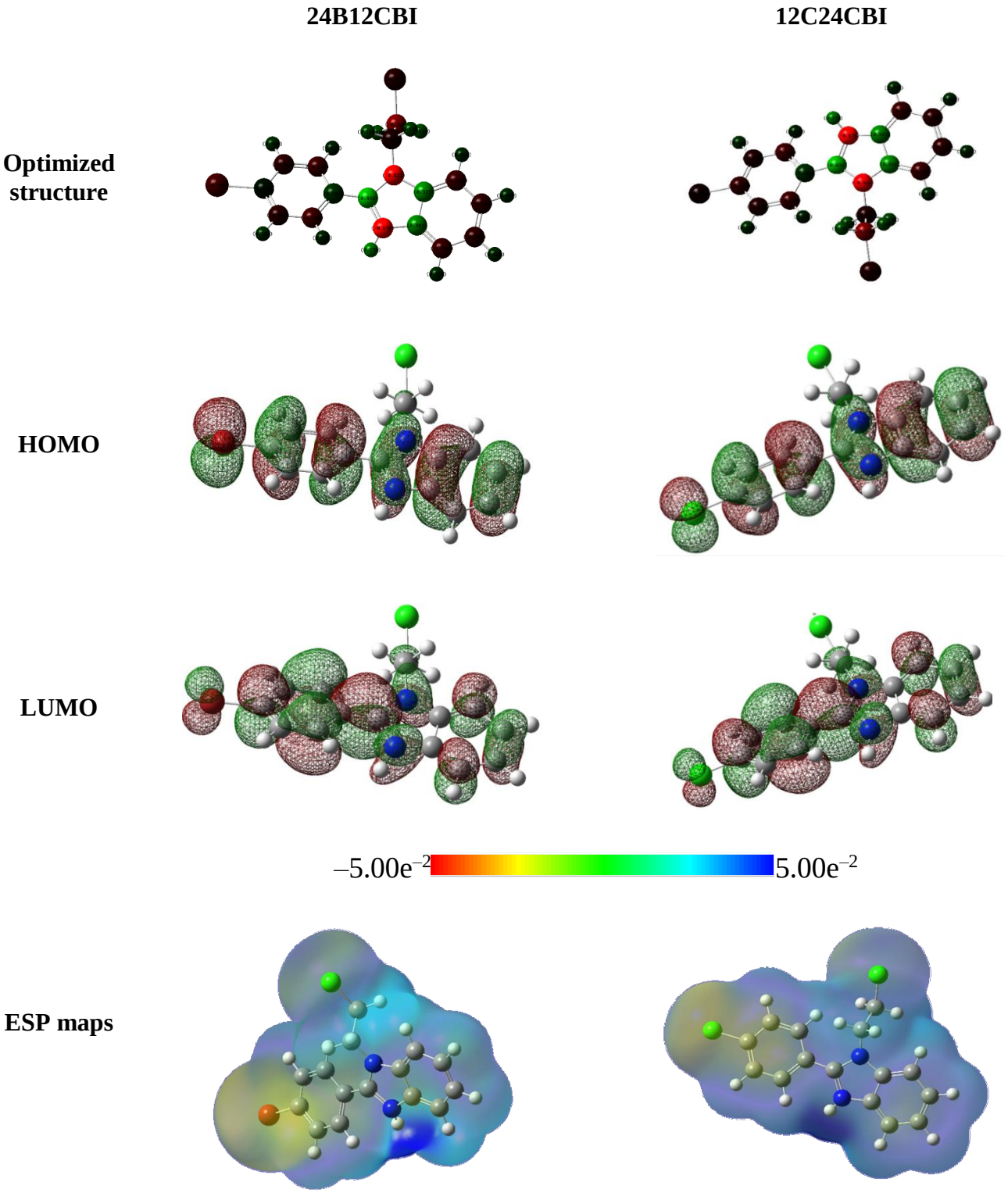

Figure 12. Optimized structures, HOMO and LUMO, and ESP maps for the studied compound in neutral form at B3LYP/6–311G++ (d,p).

It is common knowledge that the energy of frontier orbitals, specifically the LUMO and HOMO, is a significant indicator that can clarify the adsorption capability of the molecules under study. The reduced value of ΔE Equation 4 can be attributed to the low energy required to extract an electron from the HOMO of the electron-donating species to the LUMO of the electron acceptor, thus facilitating the adsorption of these molecules.

The fraction of electrons transferred (ΔN_{110}) from 24B12CBI and 12C24CBI to the Fe (110) surface was calculated using Equation 10, where the Fe (110) plane was assumed to be the most stable plane.

The work function Φ represents the theoretical value of the electronegativity in the (110) plane of iron ($\Phi=\chi(Fe110)=4.82$ eV), and the global hardness corresponds to the metallic bulk ($\eta(Fe)=0$ eV).

These descriptors indicate that 24B12CBI and 12C24CBI are reactive, which is also confirmed with the electrophilicity index since it has a high value. Finally, all descriptors suggested that 24B12CBI and 12C24CBI performed well.

Table 7. Quantum chemical descriptors for 24B12CBI and 12C24CBI obtained with DFT, B3LYP/6-311G++(d,p).

Descriptors	**24B12CBI**	**12C24CBI**
E_{HOMO} (eV)	–3.3059	–3.2988
E_{LUMO} (eV)	–0.3340	–0.3297
ΔE (eV)	2.9719	2.9692
σ (eV^{-1})	0.6730	0.6736
η (eV)	1.4859	1.4846
χ (eV)	1.8200	1.8142
μ (D)	4.4738	4.5021
ΔN	1.0095	1.0123
ω (eV)	–1.6561	–1.6457
ε (eV^{-1})	–0.6038	–0.6076
Total energy (a.u.)	–3720.8263	–1609.3172

3.2.2. Molecular dynamics

The development of mathematical approaches, including molecular dynamics (MD) simulations, can help to anticipate and explain the adsorption position of molecules on surfaces [49]. The current research was conducted to investigate just how the 24B12CBI and 12C24CBI molecules operate on the Fe (110) atomic support. The best special adsorption representation of the two systems is described in Figures 13 and 14. As shown in the two figures, both molecules fully adsorb and occupy a large part of the Fe (110) surface to reduce

the corrosion rate due to the corrosive environment. This adsorption feature suggests that there is multiple active acceptor/donor sites which contribute to the improved inhibition efficacy of the substance mentioned.

The $E_{interaction}$ values are defined by Equation 15 [50]:

$$E_{interaction} = E_{total} - (E_{surface} + E_{solution} + E_{inhibitor}) \quad (15)$$

The low value of $E_{interaction}$ attests to interaction of the molecules studied with Fe (110) atoms [51]. The values of $E_{interaction}$ for the both systems are calculated, a more negative value for 24B12CBI/Fe(110) ($-1027.478\ kJ \cdot mol^{-1}$) than for 12C24CBI/Fe(110) ($-1020.587\ kJ \cdot mol^{-1}$) reflects the best interaction between 24B12CBI and Fe(110). Consequently, these simulation results do not corroborate the results achieved by DFT and the experimental study.

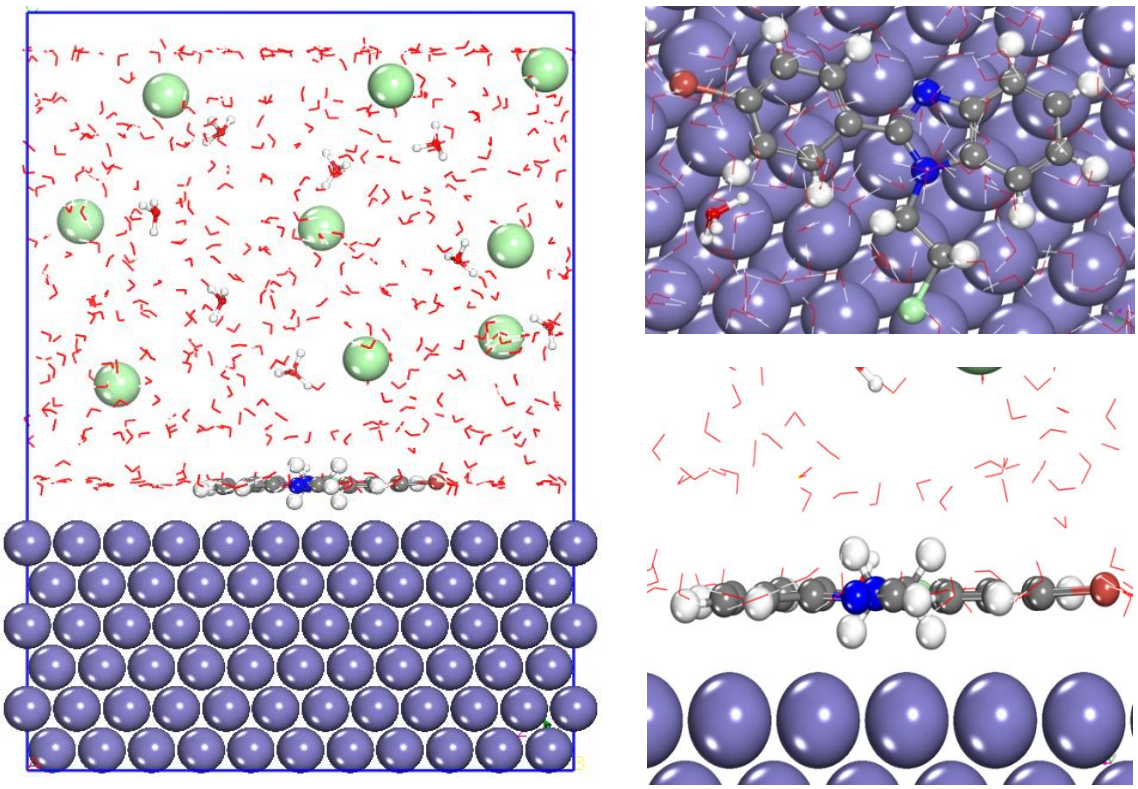

Figure 13. Side and top views of the 24B12CBI/Fe(110) system.

The radial distribution function (RDF) method was used to provide a better insight into the nature of the bonds between the both inhibitors and Fe atoms. The interfacial interatomic distance N, Cl, Br–Fe is well defined by this approach [52]. The published literature confirmed that the likelihood of chemical adsorption was higher when the bond length was less than 3.5 Å. By contrast, physical adsorption is more probable [53]. In Figure 15, the spectral data from this method are illustrated. The first peaks reveal that the bond lengths are less than 3.5 Å except Fe-Cl17 for 12C24CBI-Fe(110).

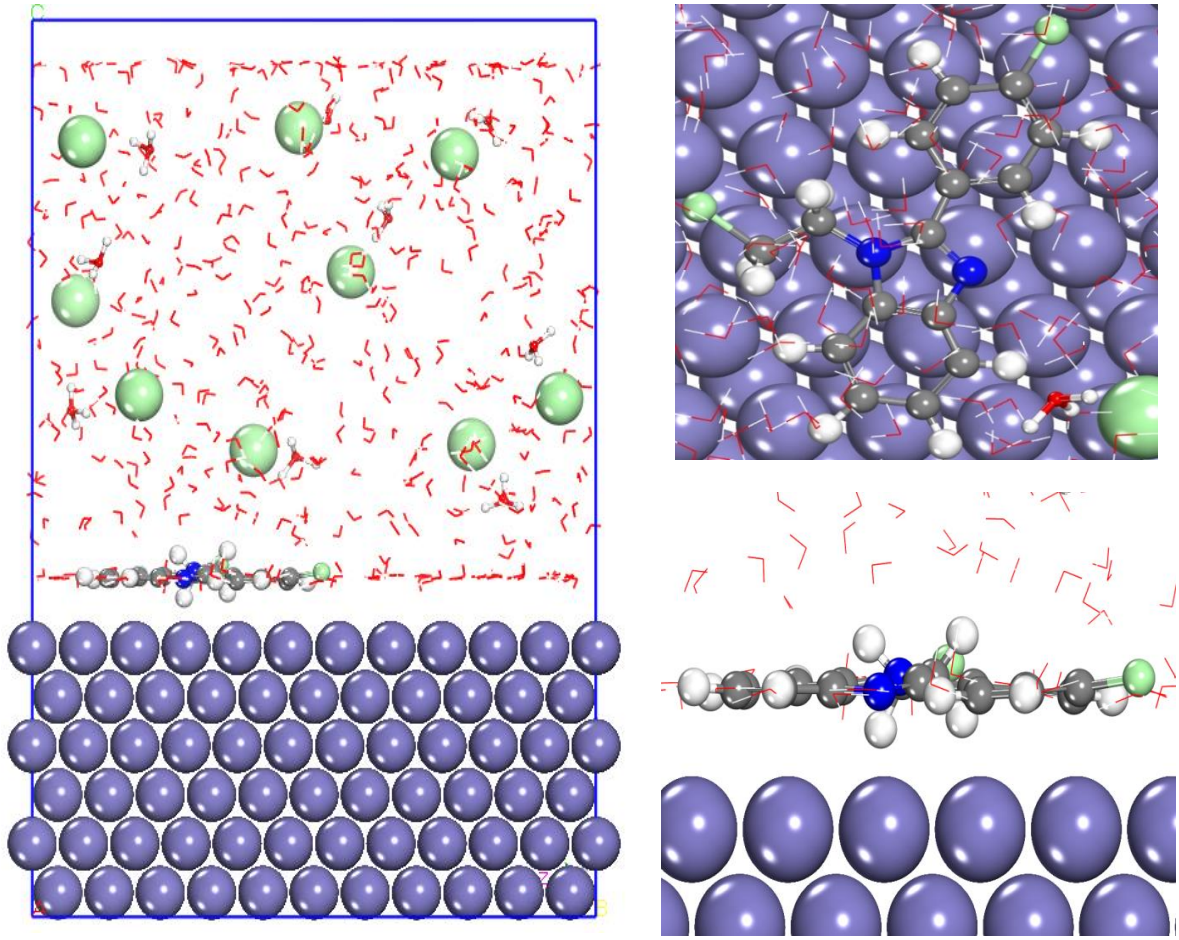

Figure 14. Side and top views of the 12C24CBI/Fe(110) system.

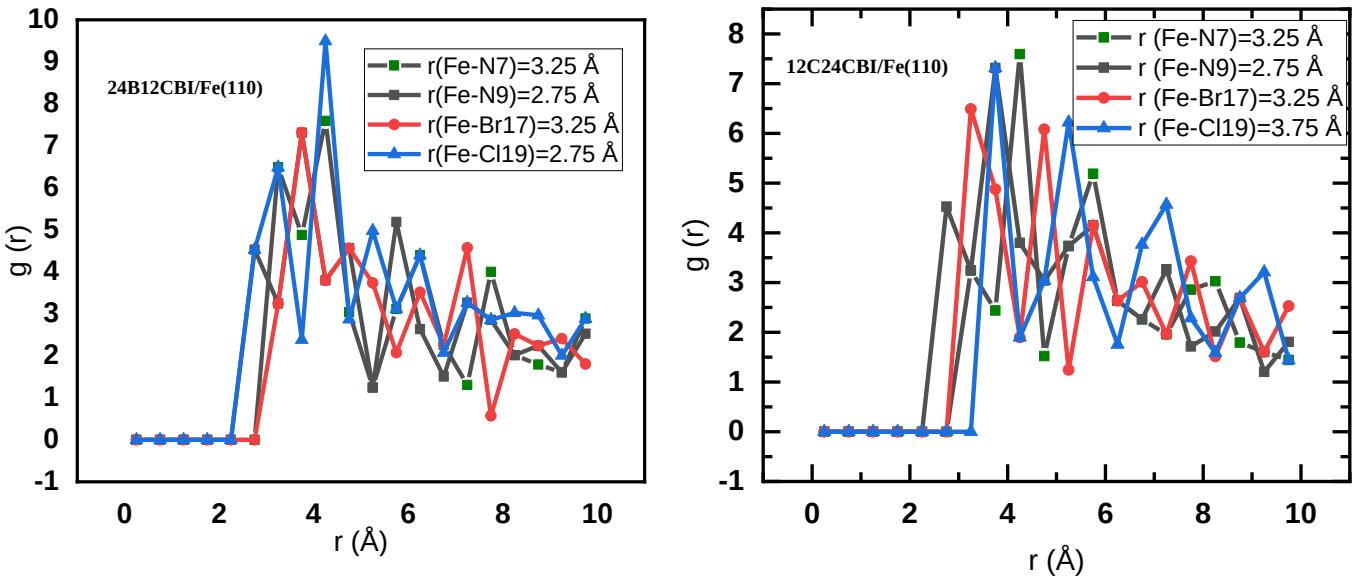

Figure 15. RDF of the 24B12CBI-Fe(110) and 12C24CBI-Fe(110).

4. Conclusions

This study aimed to evaluate the efficiency of 24B12CBI and 12C24CBI inhibition on MS in a 1 M HCl medium using electrochemical measurements, SEM/EDX analysis, and theoretical studies. Potentiodynamic polarization curves showed that inhibitors act as mixed-type inhibitors, and their inhibition efficiency increases with concentration. The maximum inhibition efficiency was 90% at 10^{-3} M for 24B12CBI and 94% for 12C24CBI. EIS diagrams showed one capacitive loop, which increased in diameter with increasing inhibitor concentration owing to the formation of a protective layer on the surfaces. The 24B12CBI and 12C24CBI molecules were found to have physisorption mechanisms according to the Langmuir isotherm. Additionally, the performance of the molecules was found to be dependent on the temperature and immersion time, with inhibition efficiency decreasing to 89.6% at 12 h for 24B12CBI after an initial increase and decreasing to 84.5% for 12C24CBI. SEM/EDX analysis confirmed the formation of a protective layer on the metal surfaces and validated the electrochemical measurements.

References

1. K. Cherrak, M. El Massaoudi, H. Outada, M. Taleb, H. Lgaz, A. Zarrouk, S. Radi and A. Dafali, Electrochemical and theoretical performance of new synthetized pyrazole derivatives as promising corrosion inhibitors for mild steel in acid environment: Molecular structure effect on efficiency, *J. Mol. Liq.*, 2021, **342**, 117507. doi: 10.1016/J.MOLLIQ.2021.117507
2. M. Barrahi, H. Elhartiti, A. El Mostaphi, N. Chahboun, M. Saadouni, R. Salghi, A. Zarrouk and M. Ouhssine, Corrosion inhibition of mild steel by Fennel seeds (*Foeniculum vulgare* Mill) essential oil in 1 M hydrochloric acid solution, *Int. J. Corros. Scale Inhib*., 2019, **8**, no. 4, 937–953. doi: 10.17675/2305-6894-2019-8-4-9
3. Y. Stiadi, M. Efdi and H. Aziz, *Gleichenia linearis* Burm. Leaf extract as corrosion inhibitor of mild steel in hydrochloric acid medium, *Int. J. Corros. Scale Inhib*., 2020, **9**, no. 4, 1498–1515. doi: 10.17675/2305-6894-2020-9-4-20
4. C.D. Fernández-Solis, A. Vimalanandan, A. Altin, J.S. Mondragón-Ochoa, K. Kreth, P. Keil and A. Erbe, Fundamentals of electrochemistry, corrosion and corrosion protection, *Soft Matter at Aqueous Interfaces*, 2016, 29–70. doi: 10.1007/978-3-319-24502-7_2
5. W. Fürbeth, Special Issue: Advanced Coatings for Corrosion Protection, *Materials*, 2020, **13**, no. 15, 3401. doi: 10.3390/MA13153401
6. M. Attarchi, A. Brenna and M. Ormellese, Cathodic protection and DC non-stationary anodic interference, *J. Nat. Gas Sci. Eng*., 2020, **82**, 103497. doi: 10.1016/J.JNGSE.2020.103497
7. G. Zhang, L. Wu, A. Tang, X.B. Chen, Y. Ma, Y. Long, P. Peng, X. Ding, H. Pan and F. Pan, Growth behavior of MgAl-layered double hydroxide films by conversion of

anodic films on magnesium alloy AZ31 and their corrosion protection, *Appl. Surf. Sci*., 2018, **456**, 419–429. doi: 10.1016/J.APSUSC.2018.06.085
8. M. Fedel, J. Franch and S. Rossi, Effect of thickness and sealing treatments on the corrosion protection properties of anodic oxide coatings on AA5005, *Surf. Coat. Technol*., 2021, **408**, 126761. doi: 10.1016/J.SURFCOAT.2020.126761
9. A.H. Ettefagh, S. Guo and J. Raush, Corrosion performance of additively manufactured stainless steel parts: A review, *Addit. Manuf*., 2021, **37**, 101689. doi: 10.1016/J.ADDMA.2020.101689
10. V.K. Bupesh Raja, K. Palanikumar, R.R. Renish, A.N. Ganesh Babu, J. Varma and P. Gopal, Corrosion resistance of corten steel – A review, *Mater. Today: Proc*., 2021, **46**, no. 9, 3572–3577. doi: 10.1016/J.MATPR.2021.01.334
11. C.L. Kugelmeier, M.R. Monteiro, R. da Silva, S.E. Kuri, V.L. Sordi and C.A. Della Rovere, Corrosion behavior of carbon steel, stainless steel, aluminum and copper upon exposure to biodiesel blended with petrodiesel, *Energy*, 2021, **226**, 120344. doi: 10.1016/J.ENERGY.2021.120344
12. Y.L. Kobzar and K. Fatyeyeva, Ionic liquids as green and sustainable steel corrosion inhibitors: Recent developments, *Chem. Eng. J*., 2021, **425**, 131480. doi: 10.1016/J.CEJ.2021.131480
13. A. Zomorodian, R. Bagonyi and A. Al-Tabbaa, The efficiency of eco-friendly corrosion inhibitors in protecting steel reinforcement, *J. Building Eng*., 2021, **38**, 102171. doi: 10.1016/J.JOBE.2021.102171
14. L. Xiong, P. Wang, Z. He, Q. Chen, J. Pu and R. Zhang, Corrosion behaviors of Q235 carbon steel under imidazoline derivatives as corrosion inhibitors: Experimental and computational investigations, *Arabian J. Chem*., 2021, **14**, no. 2, 102952. doi: 10.1016/J.ARABJC.2020.102952
15. D.S. Chauhan, P. Singh and M.A. Quraishi, Quinoxaline derivatives as efficient corrosion inhibitors: Current status, challenges and future perspectives, *J. Mol. Liq*., 2020, **320**, 114387. doi: 10.1016/j.molliq.2020.114387
16. H.M. Abd El-Lateef, K. Shalabi and A.A. Abdelhamid, One-pot synthesis of novel triphenyl hexyl imidazole derivatives catalyzed by ionic liquid for acid corrosion inhibition of C1018 steel: Experimental and computational perspectives, *J. Mol. Liq*., 2021, **334**, 116081. doi: 10.1016/J.MOLLIQ.2021.116081
17. E.B. Caldona, M. Zhang, G. Liang, T.K. Hollis, C.E. Webster, D.W. Smith and D.O. Wipf, Corrosion inhibition of mild steel in acidic medium by simple azole-based aromatic compounds, *J. Electroanal. Chem*., 2021, **880**, 114858. doi: 10.1016/J.JELECHEM.2020.114858
18. A. Farhadian, S.A. Kashani, A. Rahimi, E.E. Oguzie, A.A. Javidparvar, S.C. Nwanonenyi, S. Yousefzadeh and M.R. Nabid, Modified hydroxyethyl cellulose as a highly efficient eco-friendly inhibitor for suppression of mild steel corrosion in a 15%

HCl solution at elevated temperatures, *J. Mol. Liq.*, 2021, **338**, 116607. doi: 10.1016/J.MOLLIQ.2021.116607
19. A. El Aatiaoui, M. Koudad, T. Chelfi, S. Erkac, M. Azzouzi, A. Aouniti, K. Savaş, M. Kaddouri, N. Benchat and A. Oussaid, Experimental and theoretical study of new Schiff bases based on imidazo(1,2-a)pyridine as corrosion inhibitor of mild steel in 1 M HCl, *J. Mol. Struct*., 2021, **1226**, 129372. doi: 10.1016/J.MOLSTRUC.2020.129372
20. A. Ammazzalorso, M. Gallorini, M. Fantacuzzi, N. Gambacorta, B. De Filippis, L. Giampietro, C. Maccallini, O. Nicolotti, A. Cataldi and R. Amoroso, Design, synthesis and biological evaluation of imidazole and triazole-based carbamates as novel aromatase inhibitors, *Eur. J. Med. Chem*., 2021, **211**, 113115. doi: 10.1016/J.EJMECH.2020.113115
21. S. Li, B. Wu, X. Zheng, C. Wang, J. Zhao, H. Sun, X. Sun, Z. Tang, H. Yuan, L. Chen and X. Ma, Synthesis and biological activity of imidazole group-substituted arylaminopyrimidines (IAAPs) as potent BTK inhibitors against B-cell lymphoma and AML, *Bioorg. Chem*., 2021, **106**, 104385. doi: 10.1016/J.BIOORG.2020.104385
22. M. Talari, S. Mozafari Nezhad, S.J. Alavi, M. Mohtashamipour, A. Davoodi and S. Hosseinpour, Experimental and computational chemistry studies of two imidazole-based compounds as corrosion inhibitors for mild steel in HCl solution, *J. Mol. Liq*., 2019, **286**, 110915. doi: 10.1016/J.MOLLIQ.2019.110915
23. M. Ouakki, M. Galai, M. Rbaa, A.S. Abousalem, B. Lakhrissi, M.E. Touhami and M. Cherkaoui, Electrochemical, thermodynamic and theoretical studies of some imidazole derivatives compounds as acid corrosion inhibitors for mild steel, *J. Mol. Liq*., 2020, **319**, 114063. doi: 10.1016/J.MOLLIQ.2020.114063
24. M. Caricato, A. Frisch, J. Hiscocks and M.J. Frisch, *Gaussian 09: IOps Reference*, 2009.
25. M. Chafiq, A. Chaouiki, M.R. Al-Hadeethi, R. Salghi, A.H. Ismat, M.K. Shaaban and I.M. Chung, A joint experimental and theoretical investigation of the corrosion inhibition behavior and mechanism of hydrazone derivatives for mild steel in HCl solution, *Colloids Surf., A*, 2021, **610**, 125744. doi: 10.1016/J.COLSURFA.2020.125744
26. A.M. Abuelela, M.A. Bedair, W.M. Zoghaib, L.D. Wilson and T.A. Mohamed, Molecular structure and mild steel/HCl corrosion inhibition of 4,5-Dicyanoimidazole: Vibrational, electrochemical and quantum mechanical calculations, *J. Mol. Struct*., 2021, **1230**, 129647. doi: 10.1016/J.MOLSTRUC.2020.129647
27. A. Saady, Z. Rais, F. Benhiba, R. Salim, K. Ismaily Alaoui, N. Arrousse, F. Elhajjaji, M. Taleb, K. Jarmoni, Y. Kandri Rodi, I. Warad and A. Zarrouk, Chemical, electrochemical, quantum, and surface analysis evaluation on the inhibition performance of novel imidazo[4,5-b] pyridine derivatives against mild steel corrosion, *Corros. Sci*., 2021, **189**, 109621. doi: 10.1016/J.CORSCI.2021.109621
28. H.C. Andersen, Molecular dynamics simulations at constant pressure and/or temperature, *J. Chem. Phys*., 1980, **72**, no. 4, 2384–2393. doi: 10.1063/1.439486

29. A. Rahimi, M. Abdouss, A. Farhadian, L. Guo and J. Neshati, Development of a Novel Thermally Stable Inhibitor Based on Furfuryl Alcohol for Mild Steel Corrosion in a 15% HCl Medium for Acidizing Application, *Ind. Eng. Chem. Res*., 2021, **60**, no. 30, 11030–11044. doi: 10.1021/acs.iecr.1c01946
30. F. Kaya, R. Solmaz and İ. Halil Geçibesler, The use of methanol extract of Rheum Ribes (Işgın) flower as a natural and promising corrosion inhibitor for mild steel protection in 1 M HCl solution, *J. Ind. Eng. Chem*., 2023, **122**, 102–117. doi: 10.1016/J.JIEC.2023.02.013
31. N.A. Abdul-Rida, M.H. Sayyah and Q.A.H. Jaber, Synthesis, characterization, efficiency evaluation of some novel triazole derivatives as acid corrosion inhibitors, *Int. J. Corros. Scale Inhib*., 2023, **12**, no. 1, 101–125. doi: 10.17675/2305-6894-2023-12-1-6
32. H.I. Salman and M.J. Manshad, Inhibitive Action of Cresol Red Dye on the Corrosion of Mild Steel Alloy in 1 M H_2SO_4, *AIP Conf. Proc*., 2023, **2414**, no. 1, 050015. doi: 10.1063/5.0114864
33. N. Rajamohan, F.S.Z.S. Al Shibli, M. Rajasimman and Y. Vasseghian, Eco-friendly biomass from Ziziphus spina-christi for protection of carbon steel in acidic conditions – Parameter effects and corrosion mechanism studies, *Chemosphere*, 2022, **291**, 132756. doi: 10.1016/J.CHEMOSPHERE.2021.132756
34. M. Mobin, R. Aslam, R. Salim and S.B. Kaya, An investigation on the synthesis, characterization and anti-corrosion properties of choline based ionic liquids as novel and environmentally friendly inhibitors for mild steel corrosion in 5% HCl, *J. Colloid Interface Sci*., 2022, **620**, 293–312. doi: 10.1016/j.jcis.2022.04.036
35. Q. Wang, H. Zheng, C. Zhao, Q. Zhang, L. Liu, X. Wu, R. Zhang, Y. Sun, Z. Yan and X. Li, Experimental and theoretical insights into *Oxalis corniculata* L. extract as a sustainable and eco–friendly corrosion inhibitor for carbon steel in acidic environments, *Mater. Chem. Phys*., 2023, **306**, 128075. doi: 10.1016/J.MATCHEMPHYS.2023.128075
36. A. Chaouiki, M. Chafiq, M. Rbaa, R. Salghi, B. Lakhrissi, I.H. Ali, S. Bashir and I.M. Chung, Comprehensive assessment of corrosion inhibition mechanisms of novel benzimidazole compounds for mild steel in HCl: An experimental and theoretical investigation, *J. Mol. Liq*., 2020, **320**, 114383. doi: 10.1016/J.MOLLIQ.2020.114383
37. G.A. Benabdallah, H. Kouri, N. Labjar, K. Bouiti, E.M. Bouissoui, A. Dahrouch and S. El Hajjaji, Eco-friendly *Pistacia lentiscus* leaves extract corrosion inhibitor for C38 steel in 1 M HCl, *Int. J. Corros. Scale Inhib*., 2023, **12**, no. 1, 292–308. doi: 10.17675/2305-6894-2023-12-1-17
38. T.A. Salman, A.A. Al-Amiery, L.M. Shaker, A.A.H. Kadhum and M.S. Takriff, A study on the inhibition of mild steel corrosion in hydrochloric acid environment by 4-methyl-2-(pyridin-3-yl)thiazole-5-carbohydrazide, *Int. J. Corros. Scale Inhib*., 2019, **8**, no. 4, 1035–1059. doi: 10.17675/2305-6894-2019-8-4-14

39. J. Aslam, R. Aslam, I.H. Lone, N.R.E. Radwan, M. Mobin, A. Aslam, M. Parveen, A.A. Al-Freedi and A.A. Alzulaibani, Inhibitory effect of 2-Nitroacridone on corrosion of low carbon steel in 1 M HCl solution: An experimental and theoretical approach, *J. Mater. Res. Technol*., 2020, **9**, no. 3, 4061–4075. doi: 10.1016/J.JMRT.2020.02.033
40. N.H. Alharthi, M.A. El-Hashemy, W.M. Derafa, I.O. Althobaiti and H.A. Altaleb, Corrosion inhibition of mild steel by highly stable polydentate schiff base derived from 1,3- propanediamine in aqueous acidic solution, *J. Saudi Chem. Soc*., 2022, **26**, no. 4, 101501. doi: 10.1016/J.JSCS.2022.101501
41. M.B. Kannan, M. Rahuma, H. Khakbaz and R. Melchers, Antipsychotic drug waste: A potential corrosion inhibitor for mild steel in the oil and gas industry, *Waste Manage*., 2022, **145**, 38–47. doi: 10.1016/J.WASMAN.2022.04.029
42. A.H. Mostafatabar, A. Dehghani, P. Ghahremani, G. Bahlakeh and B. Ramezanzadeh, Molecular-dynamic/DFT-electronic theoretical studies coupled with electrochemical investigations of the carrot pomace extract molecules inhibiting potency toward mild steel corrosion in 1 M HCl solution, *J. Mol. Liq*., 2022, **346**, 118344. doi: 10.1016/J.MOLLIQ.2021.118344
43. M. Chafiq, A. Chaouiki, M.R. Al-Hadeethi, I.H. Ali, S.K. Mohamed, K. Toumiat and R. Salghi, Naproxen-Based Hydrazones as Effective Corrosion Inhibitors for Mild Steel in 1.0 M HCl, *Coatings*, 2020, **10**, no. 7, 700. doi: 10.3390/COATINGS10070700
44. O.M. Fayomi, H.F. Chahul, D.C. Ike, G.I. Ndukwe and I.M. Phoebe, Thermodynamic and Adsorption Study of the Corrosion Inhibition of Mild Steel by Aframomum chrysanthum Extract in 0.1 M Hydrochloric Acid Solution, *Asian J. Appl. Chem. Res*., 2021, **8**, no. 4, 64–73. doi: 10.9734/AJACR/2021/V8I430200
45. P. Vashishth, H. Bairagi, R. Narang, S.K. Shukla and B. Mangla, Thermodynamic and electrochemical investigation of inhibition efficiency of green corrosion inhibitor and its comparison with synthetic dyes on MS in acidic medium, *J. Mol. Liq*., 2022, **365**, 120042. doi: 10.1016/J.MOLLIQ.2022.120042
46. A.O. Okewale and O.A. Adesina, Kinetics and thermodynamic study of corrosion inhibition of mild steel in 1.5 M HCl medium using cocoa leaf extract as inhibitor, *J. Appl. Sci. Environ. Manage*., 2020, **24**, no. 1, 37–47. doi: 10.4314/JASEM.V24I1.6
47. S.A.A. Maged, R.A. Anaee and M.T. Mathew, Negative effect of calcium tablets on the corrosion of a Co–Cr–Mo alloy as an implant, *Int. J. Corros. Scale Inhib*., 2023, **12**, no. 1, 275–291. doi: 10.17675/2305-6894-2023-12-1-16
48. M. Ouakki, M. Galai, Z. Benzekri, Z. Aribou, E. Ech-chihbi, L. Guo, K. Dahmani, K. Nouneh, S. Briche, S. Boukhris and M. Cherkaoui, A detailed investigation on the corrosion inhibition effect of by newly synthesized pyran derivative on mild steel in 1.0 M HCl: Experimental, surface morphological (SEM-EDS, DRX& AFM) and computational analysis (DFT & MD simulation), *J. Mol. Liq*., 2021, **344**, 117777. doi: 10.1016/J.MOLLIQ.2021.117777

49. F. Benhiba, R. Hsissou, K. Abderrahim, H. Serrar, Z. Rouifi, S. Boukhris, G. Kaichouh, A. Bellaouchou, A. Guenbour, H. Oudda, I. Warad and A. Zarrouk, Development of New Pyrimidine Derivative Inhibitor for Mild Steel Corrosion in Acid Medium, *J. Bio-Tribo- Corros*., 2022, **8**, 1–15. doi: 10.1007/S40735-022-00637-5
50. A. Attou, M. Tourabi, A. Benikdes, O. Benali, H.B. Ouici, F. Benhiba, A. Zarrouk, C. Jama and F. Bentiss, Experimental studies and computational exploration on the 2-amino-5-(2-methoxyphenyl)-1,3,4-thiadiazole as novel corrosion inhibitor for mild steel in acidic environment, *Colloids Surf., A*, 2020, **604**, 125320. doi: 10.1016/J.COLSURFA.2020.125320
51. M. Goyal, H. Vashisht, A. Kumar, S. Kumar, I. Bahadur, F. Benhiba and A. Zarrouk, Isopentyltriphenylphosphonium bromideionic liquid as a newly effective corrosion inhibitor on metal-electrolyte interface in acidic medium: Experimental, surface morphological (SEM-EDX & AFM) and computational analysis, *J. Mol. Liq*., 2020, **316**, 113838. doi: 10.1016/J.MOLLIQ.2020.113838
52. F. Benhiba, R. Hsissou, Z. Benzikri, S. Echihi, J. El-Blilak, S. Boukhris, A. Bellaouchou, A. Guenbour, H. Oudda, I. Warad, N.K. Sebbar and A. Zarrouk, DFT/electronic scale, MD simulation and evaluation of 6-methyl-2-(p-tolyl)-1,4-dihydroquinoxaline as a potential corrosion inhibition, *J. Mol. Liq*., 2021, **335**, 116539. doi: 10.1016/J.MOLLIQ.2021.116539
53. M. El Faydy, F. Benhiba, H. About, Y. Kerroum, A. Guenbour, B. Lakhrissi, I. Warad, C. Verma, E.S.M. Sherif, E.E. Ebenso and A. Zarrouk, Experimental and computational investigations on the anti-corrosive and adsorption behavior of 7-N,N'-dialkyaminomethyl-8-Hydroxyquinolines on C40E steel surface in acidic medium, *J. Colloid Interface Sci*., 2020, **576**, 330–344. doi: 10.1016/J.JCIS.2020.05.010

♦ ♦ ♦